

Neuronal Excitability

Automated Image Analysis Reveals Different Localization of Synaptic Gephyrin C4 Splice Variants

Filip Liebsch,¹ Fynn R. Eggersmann,² Yvonne Merkler,¹ Peter Kloppenburg,² and Günter Schwarz³<https://doi.org/10.1523/ENEURO.0102-22.2022>

¹Institute of Biochemistry, Department of Chemistry, University of Cologne, Cologne 50674, Germany, ²Biocenter, Institute for Zoology, and Cologne Excellence Cluster on Cellular Stress Responses in Aging-Associated Diseases (CECAD), University of Cologne, Cologne 50674, Germany, and ³Institute of Biochemistry, Department of Chemistry, Center for Molecular Medicine Cologne (CMMC), University of Cologne, Cologne 50674, Germany

Abstract

Postsynaptic scaffolding proteins function as central organization hubs, ensuring the synaptic localization of neurotransmitter receptors, trans-synaptic adhesion proteins, and signaling molecules. Gephyrin is the major postsynaptic scaffolding protein at glycinergic and a subset of GABAergic inhibitory synapses. In contrast to cells outside the CNS, where one gephyrin isoform is predominantly expressed, neurons express different splice variants. In this study, we characterized the expression and scaffolding of neuronal gephyrin isoforms differing in the inclusion of the C4 cassettes located in the central C-domain. In hippocampal and cortical neuronal populations, gephyrin P1, lacking additional cassettes, is the most abundantly expressed isoform. In addition, alternative splicing generated isoforms carrying predominantly C4a, and minor amounts of C4c or C4d cassettes. We detected no striking difference in C4 isoform expression between different neuron types and a single neuron can likely express all C4 isoforms. To avoid the cytosolic aggregates that are commonly observed upon exogenous gephyrin expression, we used adeno-associated virus (AAV)-mediated expression to analyze the scaffolding behavior of individual C4 isoforms in murine dissociated hippocampal glutamatergic neurons. While all isoforms showed similar clustering at GABAergic synapses, a thorough quantitative analysis revealed localization differences for the C4c isoform (also known as P2). Specifically, synaptic C4c isoform clusters showed a more distal dendritic localization and reduced occurrence at P1-predominating synapses. Additionally, inhibitory currents displayed faster decay kinetics in the presence of gephyrin C4c compared with P1. Therefore, inhibitory synapse heterogeneity may be influenced, at least in part, by mechanisms relating to C4 cassette splicing.

Key words: adeno-associated virus; automated image analysis; gephyrin; inhibitory synapses; splice variants

Significance Statement

A neuron receives and integrates thousands of different synaptic inputs. At synapses of the same type, i.e., using the same neurotransmitter, subtle differences in their molecular composition could account for functional changes. Diverse synapse populations could contain different isoforms of the same protein, which are themselves generated by alternative splicing. In this work, we focused on the neuronal isoforms of gephyrin, which organizes structures at most inhibitory synapses. While overall similar properties of all isoforms were observed, an in-depth automated analysis revealed that the localization of clusters from one of the isoforms was different. Finally, this indicates that the alternative splicing of gephyrin could be one of the factors influencing the organization of postsynaptic proteins at diverse synapse populations.

Introduction

The postsynaptic side of neuronal synapses contains scaffolding proteins that keep neurotransmitter receptors, trans-synaptic adhesion molecules and additional functional elements with precise stoichiometries in place (Sheng and Kim, 2011). Gephyrin (Gphn), initially co-purified with glycine receptors (GlyRs), is an important postsynaptic scaffolding protein at inhibitory glycinergic and GABAergic synapses (Prior et al., 1992; Fritschy et al., 2008). It is ubiquitously expressed and in addition to its neuronal role, the protein serves a more “ancient” metabolic function in molybdenum cofactor biosynthesis throughout the whole body (Feng et al., 1998; Stallmeyer et al., 1999). Both Gphn functions are essential for postnatal survival (Feng et al., 1998; Grosskreutz et al., 2003; O’Sullivan et al., 2016).

Gphn consists of an N-terminal G-domain that has the propensity to trimerize and a C-terminal E-domain with the ability to dimerize and directly interact with the cytosolic loop of the GlyR β -subunit (Schwarz et al., 2001; Schrader et al., 2004; Sola et al., 2004). The terminal domains are connected by the central C-domain, which provides structural flexibility (Belaidi and Schwarz, 2013) and regulates fine-tuning of postsynaptic clustering of glycine receptors and GABA_A receptors (GABA_ARs) via protein-protein interactions and posttranslational modifications (Tyagarajan et al., 2011, 2013; Sander et al., 2013; Dejanovic et al., 2014b).

Since its discovery, multiple Gphn isoforms have been described in rodents and humans (Prior et al., 1992; Kirsch et al., 1993; Heck et al., 1997; Ramming et al., 2000; David-Watine, 2001; Rees et al., 2003). The murine gephyrin gene (*Gphn*) was originally described to consist of 29 exons (Heck et al., 1997; Meier et al., 2000; Ramming et al., 2000; Fritschy et al., 2008). A recent targeted approach, together with long-read sequencing, discovered 40 exons, and alternative splicing results in the expression of 277 unique transcripts (Dos Reis et al., 2022). The major gephyrin isoform in the brain is referred to as P1 and is generated from 22 exons (Prior et al., 1992; Fritschy et al., 2008; Dos Reis et al., 2022). The P1 open reading frame of human

GPHN is 94% homologous to the rodent one, which translates to 99.7% amino acid conservation (Rees et al., 2003). All internal exons may undergo alternative splicing (Dos Reis et al., 2022) and traditionally certain exons were named according to the resulting alternative sequences in either of the three protein domains, e.g., G2, C3, C4a, C4c, C4d, and E2 (Fritschy et al., 2008; Fig. 1a).

The inclusion of the G2 cassette results in a dominant-negative effect on GlyR clustering and prevents the enzyme’s ability to synthesize the molybdenum cofactor (Meier et al., 2000; Bedet et al., 2006; Smolinsky et al., 2008). The C3 cassette is mainly expressed in glial cells and tissues outside the brain; it is excluded from transcripts through NOVA proteins, neuronal regulators of pre-mRNA splicing (Ule et al., 2003; Licatalosi et al., 2008). Much less is known about the functional impact of C4 alternative splicing. Transcripts with C4 cassettes are predominantly found in neuronal tissue (Ramming et al., 2000; Rees et al., 2003; Smolinsky et al., 2008). The C4 cassettes can be present individually in single transcripts but are occasionally found in combination with other C4 cassettes within the same transcript (Ramming et al., 2000; Rees et al., 2003; Witte et al., 2019). In the first three postnatal weeks, exon skipping of the C4a cassette is increased, and this process is affected by the RNA-binding protein Sam68 (Witte et al., 2019). Additionally, different phosphorylation patterns were observed between P1 and C4c, when purified from insect cells (Herweg and Schwarz, 2012).

Here, we analyzed the neuronal expression and clustering of Gphn isoforms that differ in the inclusion of one of the C4 cassettes. We hypothesized that C4 isoforms could form structurally different scaffolds, which could in turn affect receptor clustering and/or synapse localization. Our results showed a relatively high abundance of C4a-containing transcripts in all major hippocampal and cortical neuron populations, while C4c and C4d were only detectable in low amounts. Interestingly, synaptic clustering in cultured neurons was similar for all C4 isoforms, suggesting that Gphn’s basic scaffolding properties remained unaltered following C4 splicing. However, an in-depth automated analysis of GABAergic synapses revealed that the addition of the C4c splice cassette resulted in more distally localized clusters. Additionally, when differentially labeled isoforms were co-expressed, we detected the largest effect between Gphn P1 and C4c variants, pointing to a unique role for the C4c-containing isoform. Functional experiments revealed that inhibitory currents displayed faster decay kinetics in the presence of gephyrin C4c compared with P1.

Materials and Methods

DNA constructs

Initially, pmEGFP-C2 was generated from pEGFP-C2 (Clontech) by introducing the point mutation L221K through site-directed mutagenesis. Plasmids pAAV-hSyn-moxBFP and pAAV-hSyn-mEGFP were generated from moxBFP (a gift from Erik Snapp, Addgene plasmid #68064; <http://n2t.net/addgene:68064>; RRID:Addgene_68064) and pAAV-hSyn-mScarlet (a gift from Karl Deisseroth, Addgene

Received March 12, 2022; accepted December 13, 2022; First published December 21, 2022.

The authors declare no competing financial interests.

Author contributions: F.L., F.R.E., Y.M., P.K., and G.S. designed research; F.L., F.R.E., and Y.M. performed research; F.L., F.R.E., and Y.M. analyzed data; F.L. and G.S. wrote the paper.

This work was supported by the Article Processing Charge from the DFG (German Research Foundation, 491454339).

Acknowledgments: We thank the Biocenter Imaging Facility and Dr. Matthias Gruhn for their support with confocal microscopy, Dr. Patricia M. G. E. Brown for scientific discussions, Dr. Franziska Neuser, Julia Reich, and Joana Stegemann for their support with primary hippocampal cultures, as well as Monika Laurien and Simona Jansen for their technical support.

Correspondence should be addressed to Filip Liebsch at f.liebsch@uni-koeln.de or Günter Schwarz at gschwarz@uni-koeln.de.

<https://doi.org/10.1523/ENEURO.0102-22.2022>

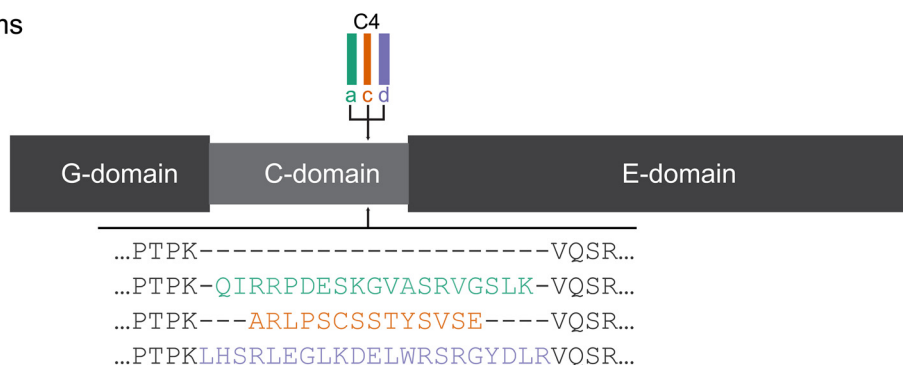
Copyright © 2023 Liebsch et al.

This is an open-access article distributed under the terms of the Creative Commons Attribution 4.0 International license, which permits unrestricted use, distribution and reproduction in any medium provided that the original work is properly attributed.

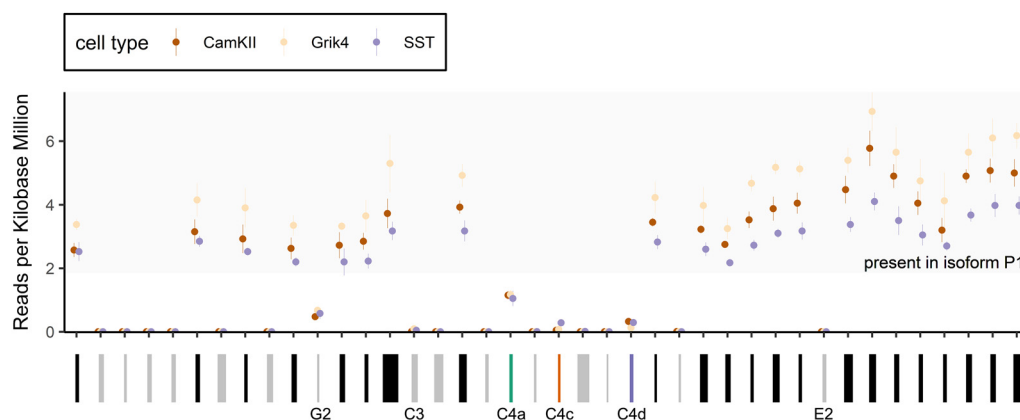
a mouse *Gphn* locus: Chromosome 12: 78,226,379-78,684,772
exon structure



C4 isoforms



b hippocampus (SPLICECODE database)



c dissociated hippocampal cultures

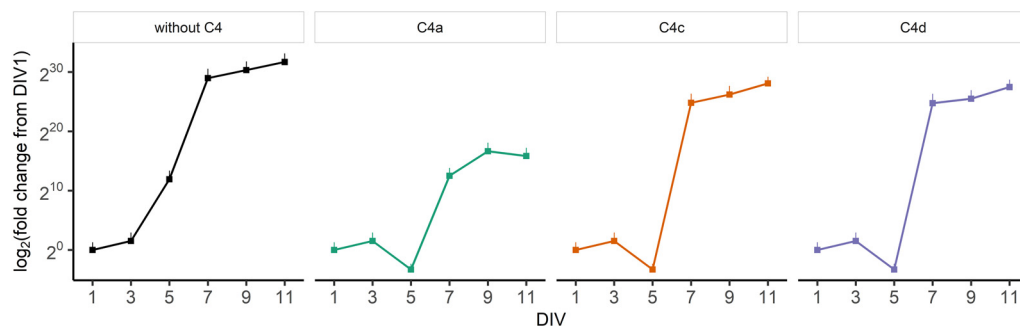


Figure 1. Alternative splicing of murine gephyrin. **a**, The *Gphn* locus consists of 40 exons. Isoform P1 is generated from 22 exons (black) and the remaining 18 (gray, green, orange, purple) can contribute to numerous variants. Alternative splicing of exons in the C4 cluster results in the insertion of short sequences (14–21 aa, sequences from *Rattus norvegicus* are indicated here) in the C-domain, i.e., C4a (green), C4c (orange), or C4d (purple). **b**, Normalized transcript expression (ribosome-associated mRNAs) in glutamatergic [Ca^{2+} /calmodulin-dependent protein kinase II (CamKII) and glutamate receptor kainate type subunit 4 (Grik4)] and GABAergic [somatostatin (SST)] neurons, isolated from the hippocampus (SPLICECODE database). See Extended Data Figure 1-1. **c**, Normalized transcript expression (housekeeping genes *Rpl2* and β -actin) of C4 cassettes in dissociated hippocampal cultures during *in vitro* development, analyzed by quantitative PCR after 1, 3, 5, 7, 9, and 11 d *in vitro* (DIV; $N=3$ independent cultures). Each data point represents the mean of all biological replicates, error bars represent standard deviation.

plasmid #131001; <http://n2t.net/addgene:131001>; RRID: [Addgene_131001](https://identifiers.org/RRID:Addgene_131001)) by PCR subcloning using BamHI and EcoRI. Next, pAAV-hSyn-moxBFP and pAAV-EF1a-mCherry-IRES-Flpo (a gift from Karl Deisseroth, Addgene plasmid #55634; <http://n2t.net/addgene:55634>; RRID: [Addgene_55634](https://identifiers.org/RRID:Addgene_55634)) were used to generate pAAV-hSyn-moxBFP-IRES-Flpo using NEBuilder HiFi DNA Assembly (NEB). Finally, pAAV-CaMKIIa-EGFP (a gift from Bryan Roth, Addgene plasmid #50469; <http://n2t.net/addgene:50469>; RRID: [Addgene_50469](https://identifiers.org/RRID:Addgene_50469)) and pAAV-hSyn-moxBFP-IRES-Flpo were used to generate pAAV-CaMKIIa-moxBFP-IRES-Flpo using NEBuilder HiFi DNA Assembly. From this template, the control pAAV-CaMKIIa-moxBFP was generated by deleting IRES-Flpo through site-directed mutagenesis.

Rat gephyrin C4c in pEGFP-C2 was previously described (Dejanovic et al., 2014a) and the gephyrin ORF was introduced into pAAV-hSyn-mScarlet or pAAV-hSyn-mEGFP by PCR subcloning using XcmI and Sall. The C4c cassette was either deleted or replaced with the C4a or C4d cassette using overlap extension PCR. These served as PCR templates to generate the inserts for Flp-dependent constructs. Plasmid backbones of pAAV-hSyn-mScarlet, excluding the mScarlet ORF and WPRE, were PCR amplified. FRT-sites and compatible overlapping ends were introduced into primers used for insert and plasmid backbone PCRs. Compatible overlapping ends were designed so that mScarlet-Gphn or mEGFP-Gphn ORFs were inverted on ligation using NEBuilder HiFi DNA Assembly.

The plasmids pAdDeltaF6 (Addgene plasmid #112867; <http://n2t.net/addgene:112867>; RRID: [Addgene_112867](https://identifiers.org/RRID:Addgene_112867)) and pAAV2/1 (Addgene plasmid #112862; <http://n2t.net/addgene:112862>; RRID: [Addgene_112862](https://identifiers.org/RRID:Addgene_112862)) were a gift from James M. Wilson.

All DNA constructs were confirmed by Sanger sequencing (Eurofins).

Primary hippocampal cultures

Dissociated primary hippocampal cultures were prepared from C57BL/6Nj embryos (E17.5) of either sex. After dissociation, 65,000 cells were seeded on Poly-L-lysine coated 13-mm cover slips (#1) or 75,000 cells per well of a Poly-L-lysine coated 24-well plate. Cultures were grown in neurobasal medium supplemented with B-27, N-2, and L-glutamine (Thermo Fisher Scientific). Cultures were transfected after 8 d *in vitro* (DIV) with 400 ng plasmid DNA using Lipofectamine 2000 according to the manufacturer's instructions. After 9 DIV, cultures were infected with a total of 2×10^8 viral genome copies (GC). Recombinant AAV2/1 particles (1:1 Mix for co-infection experiments) were diluted in neurobasal medium supplemented with B-27, N-2, and L-glutamine (Thermo Fisher Scientific) before they were added to the cultures. To adjust the osmolality of the culture medium for electrophysiology experiments, 30 mM NaCl was added on DIV11.

Transcript expression in primary hippocampal cultures

Cultures in 24-well plates were washed with PBS, harvested with a cell scraper, and resuspended in TRI reagent

(Sigma). RNA was separated from other cellular components according to the manufacturer's protocol and resuspended in 15 μ l dH₂O. In 10 μ l, 400 ng RNA, 10 μ M oligo (dT) primer, and 1 μ M dNTPs were incubated at 65°C for 5 min and then chilled on ice. The RNA-mix was added to a 10 μ l solution of RT buffer (Invitrogen), 25 mM MgCl₂, 50 mM DTT and 1 μ l SuperScript III RT (200 U/ μ l, Invitrogen). This mix was subjected to the following temperature cycle: 25°C 10 min, 50°C 60 min, 70°C 15 min, and subsequently chilled on ice. After incubation with 1 μ l RNase A at 37°C for 20 min, the samples were stored at -20°C. For quantitative PCR (qPCR), 2 μ l cDNA was added per well of a 384-well plate (Bio-Rad). A master mix, containing 2.5 μ l ORA (qPCR Green ROX H Mix, 2 \times Master) mix and 0.5 μ l of a 10 μ M mixture of forward and reverse primer, was prepared and added to each sample. The plate was sealed with Microseal Adhesive Sealer (Bio-Rad) and spun down for 20 s at 300 \times g. The plate was placed in a CFRX384 Real-Time System (Bio-Rad) and the qPCR was performed according to the ORA HighQ qPCR manual. Acquired cycle threshold (Ct) values were exported and normalized to the housekeeping control (RPL37a and Actin β). Δ Ct = Ct (gene of interest) - Ct (housekeeping gene). The fold change was calculated by dividing the 2^{Δ Ct} by 2^{Δ Ct} of the control condition.

rAAV2/1 preparation

Recombinant AAV2/1 particles were prepared in HEK293T cells (DSMZ no. ACC 635) according to the detailed protocol by (Kimura et al., 2019). Viral particles were precipitated with PEG/NaCl and subsequently cleared via chloroform extraction (Kimura et al., 2019). Purity of viral preparations were assessed with SDS-PAGE and AAV titers determined using Gel green® (Biotium) protocol (Xu et al., 2020). Fluorescence was measured at 507 \pm 5 nm excitation and 528 \pm 5 nm emission using a plate reader equipped with monochromators (Tecan Spark).

Immunocytochemistry

Cells were fixed with 4% formaldehyde in PBS for 15 min and quenched with NH₄Cl in PBS at room temperature (RT). All subsequent incubation and wash steps (PBS) were performed at RT. After blocking/permeabilization for 1 h with 10% goat serum, 1% BSA, 0.2% Triton X-100 in PBS, the following primary antibodies (Synaptic Systems) were used: anti-vesicular GABA transporter (vGAT) (1:1000, #131003) for inhibitory presynaptic terminals; anti-GABA_AR γ 2 (1:500, #224004), anti-GABA_AR α 1 (1:500, #224204), and anti-GABA_AR α 2 (1:500, #224102) for postsynaptic GABA_ARs. The following secondary antibodies were used: goat anti-rabbit AlexaFluor 488 (1:500, #A-11034, Thermo Fisher Scientific), goat anti-rabbit AlexaFluor 647 (1:500, #A-21245, Thermo Fisher Scientific), and goat anti-guinea pig AlexaFluor 647 secondary antibodies (1:500, #ab150187, Abcam). Coverslips were mounted with Mowiol/Dabco.

Confocal microscopy and image analysis

Image stacks [0.3- μ m z-step size, 3432 \times 3432 (144.77 \times 144.77 μ m)] were acquired on a Leica TCS SP8 LIGHTNING

upright confocal microscope with an HC PL APO CS2 63 \times /1.30 glycerol objective, equipped with hybrid detectors (Leica HyD) and the following diode lasers: 405, 488, 552, and 638 nm. LIGHTNING adaptive deconvolution using “Mowiol” setting were applied. This form of adaptive image reconstruction is capable of theoretical resolutions down to 120 nm (lateral) and 200 nm (axial).

Images were segmented and analyzed in an automated fashion using ImageJ/FIJI 1.53c (<https://imagej.net/software/fiji/>) and the code is freely available online at https://github.com/FilLieb/quantitative_synapse_analysis. Maximum Z projections were used for image segmentation. Rolling ball background subtraction, median filtering, and auto thresholding methods were used: Default (for vGAT and GABA_AR γ 2 masks), Otsu (for soma, GABA_AR α 1, and GABA_AR α 2 masks), and mean (for neuron mask). Gephyrin cluster masks were generated by thresholding with local maxima identification using the ImageJ/FIJI find maxima and segmented particles function (Moreno Manrique et al., 2021). Individual regions of interest were classified according to their overlap with foreground in segmented masks and filtered with appropriate size ranges. For intensity measurements, mean background intensity (as defined by the respective masks) was subtracted from average Z projections.

Electrophysiology

Whole-cell patch-clamp recordings under current clamp and voltage clamp were conducted on primary cultures of murine hippocampal neurons between DIV12 and DIV15 at 30°C. Neurons were visualized with a fixed-stage upright microscope (Axio Examiner.D1, Carl Zeiss GmbH) using a water-immersion objective (Plan-Apochromat, 40 \times , 1 numerical aperture, 2.5 mm working distance, Carl Zeiss GmbH). The microscope was equipped with fluorescence and infrared differential interference contrast optics (Dodt and Zieggländer, 1994). Red fluorescing gephyrin-positive cells were visualized with an X-Cite 120 illumination system (EXFO Photonic Solutions). Recordings were performed with an EPC9 patch-clamp amplifier (HEKA) controlled by the program PatchMaster (version 2 \times 90.5, HEKA running on Windows 10). Data were recorded using a Micro1401 data acquisition interface (Cambridge Electronic Design Limited) and Spike 2 (version 7.08, Cambridge Electronic Design Limited). Data were sampled at 20 kHz and low-pass filtered at 10 kHz with a four-pole Bessel filter. Offline, an FIR digital filter at 2 kHz was applied in Spike 2. Electrodes with tip resistances between 4 and 6 M Ω were made from borosilicate glass (0.86-mm inner diameter; 1.5-mm outer diameter; GB150-8P, Science Products) with a vertical pipette puller (PP-830, Narishige).

During the recording, neurons were continuously superfused at a flow rate of \sim 2.5 ml min⁻¹ with a carbonated (95% O₂ and 5% CO₂) extracellular saline containing (in mM): 125 NaCl, 21 NaHCO₃, 2.5 KCl, 2 MgCl₂, 1.2 NaH₂PO₄, 10 HEPES, 5 glucose, adjusted to pH 7.2 with NaOH. For the voltage clamp recordings, glutamatergic input was blocked with 5 \times 10⁻⁵ M DL-2-amino-5-phosphonopentanoic acid (DL-AP5; BN0086, Biotrend Chemikalien GmbH) and 10⁻⁵ M 6-cyano-7-nitroquinoxaline-2,3-dione (CNQX; C127, Sigma-

Aldrich). Na⁺ mediated action potentials were blocked by 10⁻⁶ M tetrodotoxin (TTX; T-550, Alomone, Jerusalem BioPark). Current-clamp recordings were performed with a pipette solution containing (in mM): 140 K-gluconate, 10 KCl, 2 MgCl₂, 10 HEPES, 0.1 EGTA, adjusted to pH 7.2 with KOH. For voltage clamp recordings of miniature IPSCs (mIPSCs), the patch pipette solution contained (in mM): 133 CsCl, 2 MgCl₂, 1 CaCl₂, 10 HEPES, 10 EGTA, adjusted with CsOH to pH 7.2. The liquid junction potential between intracellular and extracellular solution for current-clamp (14.6 mV) and voltage-clamp (6.3 mV) recordings were calculated using the LJPcalc software (<https://sw Harden.com/LJPcalc>; arXiv:1403.3640v2; <https://doi.org/10.48550/arXiv.1403.3640>) and compensated accordingly.

Neurons were voltage clamped at -50 mV. Because of the high intracellular chloride concentration, GABA_A receptor-mediated currents were detected as inward currents. Data were analyzed at 50 s intervals after the recording stabilized (\sim 10 min after obtaining whole-cell configuration). Data analysis was performed with Spike 2 (version 7.08, Cambridge Electronic Design Limited), Igor Pro 6 (version 6.37, Wavemetrics), and GraphPad Prism (version 6.01, GraphPad Software Inc.). mIPSC frequency, amplitude, and decay were determined offline. Events in voltage clamp traces were automatically detected by the Minhee Analysis program (version 1.1.3; Kim et al., 2021), when the signal crossed a threshold that was set and adjusted manually depending on the noise level of the signal. Events were classified as mIPSCs when the calculated coefficient of determination $r^2 > 0.3$ and tau 1 < τ < 300 ms. This semi-automated detection procedure was verified by visual inspection. Statistical analysis between the two splice variants was performed using a two-sided permutation test.

Statistical analysis and data visualization

Individual data points, mean, confidence intervals (CIs), and standard deviation are displayed in the figures. Estimation statistics and plots were generated with the R package DABESTR (Ho et al., 2019). Data were tested for normality, using violation of the Shapiro–Wilk test at $p < 0.01$ as the criterion. Data were analyzed for homoscedasticity, using violation of Levene’s test at $p < 0.01$. Datasets not meeting normality or homoscedasticity assumptions were analyzed using nonparametric tests (as indicated in the figure legends). All other data were analyzed with the indicated parametric tests. For imaging experiments, $N = 15$ cells per condition from three independent cultures were analyzed. For electrophysiology experiments, $N = 12$ for P1 and $N = 13$ for C4c cells from five independent cultures were analyzed.

Statistical analyses and data visualization were performed using R version 4.1.0 (2021–05–18), lsmeans v. 2.30–0, emmeans v. 1.7.2, MASS v. 7.3–54, rstatix v. 0.7.0, ggpubr v. 0.4.0, svglite v2.0.0, RcolorBrewer v. 1.1–2, ggrepel v. 0.9.1, forcats v. 0.5.1, stringr v. 1.4.0, dplyr v. 1.0.7, purrr v. 0.3.4, readr v. 2.0.0, tidyr v. 1.1.3, tibble v. 3.1.3, ggplot2 v. 3.3.5, tidyverse v. 1.3.1, rio v. 0.5.27, pacman v. 0.5.1, dabestr v.0.3.0 in Rstudio environment (<https://www.rstudio.com/>), Platform: x86_64-w64-mingw32/x64 (64-bit). Figures were

prepared with OMERO (<https://www.openmicroscopy.org/>) and Inkscape (<https://inkscape.org/>).

Ethics statement

We complied with all relevant ethical regulations for animal testing and research. Experiments were approved by the local research ethics committees (Germany, Landesamt für Natur, Umwelt und Verbraucherschutz Nordrhein-Westfalen, reference 2016.A466 and 2021.A450).

Data availability

Plasmids will be made available via Addgene (<https://www.addgene.org/>): pAAV-hSyn-fDIO-mScarlet-Gphn_P1 (Addgene plasmid # 194972), pAAV-hSyn-fDIO-mScarlet-Gphn_C4a (Addgene plasmid # 194973), pAAV-hSyn-fDIO-mScarlet-Gphn_C4c (Addgene plasmid # 194974), pAAV-hSyn-fDIO-mScarlet-Gphn_C4d (Addgene plasmid # 194975), pAAV-hSyn-fDIO-mEGFP-Gphn_P1 (Addgene plasmid # 194978), pAAV-CamKIIa-moxBFP-WPRE (Addgene plasmid # 194976), pAAV-CamKIIa-moxBFP-IRES-Flpo (Addgene plasmid # 194977).

Code accessibility

The code for automated image analysis written in ImageJ Macro Language is freely available online at https://github.com/FilLieb/quantitative_synapse_analysis. The code is available as [Extended Data 1](#). The code was run under Windows 10 × 64 (Build 19042) on an HP Pavilion Desktop PC570-p0xx.

Results

Neuronal expression of alternatively spliced Gphn transcripts

To analyze whether the sequences encoded by *Gphn* exons are part of translated transcripts (ribosome-associated mRNAs) in neurons, we retrieved their normalized expression (reads per kilobase million) from the SPLICECODE database (Furlanis et al., 2019). In hippocampal glutamatergic [Ca^{2+} /calmodulin-dependent protein kinase II (CamKII) and glutamate receptor kainate type subunit 4 (Grik4)] and GABAergic [somatostatin (SST)] neurons, transcript expression of 27 exons was detected (Fig. 1b). High reads per kilobase million were detected for the 22 exons coding for the *Gphn* isoform P1. The expression of E2 and any of the recently discovered exons (Dos Reis et al., 2022) was below the limit of detection in the dataset. The expression profile in cortical [glutamatergic; CamKII (sodium channel epithelial 1 subunit α ; Scnn1a), Grik4; and GABAergic (SST, parvalbumin; Pvalb, vasointestinal peptide; Vip)] neurons was comparable to the cells in the hippocampus (Extended Data Fig. 1-1).

By calculating the average reads per kilobase million for all cell types, we estimated that ~64% of all transcripts in hippocampal neurons encode for the isoform P1 (59% in cortical neurons). Consequently, the remainder of transcripts consisted of 10% G2 (9% in cortex), 1% C3 (1% in cortex), 19% C4a (21% in cortex), 2% C4c (4% in cortex), and 4% C4d (6% in cortex). Overall, these data suggest that in the major neuron types in the murine hippocampus

and cortex *in vivo* (Furlanis et al., 2019), most *Gphn* mRNAs code for P1 and predominantly five cassette exons can be used to generate alternatively spliced transcripts. It is important to notice that mRNA abundance correlates only partially with protein levels (Vogel and Marcotte, 2012; Smith et al., 2013; Liu et al., 2016; Aebersold et al., 2018).

The dominant-negative function of *Gphn* G2 (Bedet et al., 2006; Smolinsky et al., 2008) and reduced oligomerization as well as lower receptor affinity of the predominantly non-neuronally expressed isoform of *Gphn* C3 have been previously studied (Herweg and Schwarz, 2012; Nawrotzki et al., 2012). To gain insight into the properties of the thus far little explored *Gphn* C4 isoforms, we undertook a reductionist approach and analyzed expression and clustering of C4 isoforms in dissociated primary hippocampal cultures. The endogenous expression of transcripts coding for the different C4 isoforms increases over time in hippocampal cultures (Fig. 1c). While transcript levels without C4 increase after 5 d *in vitro* (DIV), those containing C4a, C4c, or C4d increase after 7 DIV. After 9 and 11 DIV, all transcript levels plateaued (Fig. 1c).

Overall, in agreement with previous work, *Gphn* C4 isoforms are expressed in major neuronal populations in hippocampus and cortex. In dissociated neuronal cultures, levels of *Gphn* transcripts with and without C4 cassettes increased during times of synaptogenesis (Deng et al., 2007).

Exogenous *Gphn* C4 isoforms localize to GABAergic synapses

Recombinantly expressed *Gphn* in non-neuronal and neuronal cells has the tendency to form cytosolic aggregates, in the field often referred to as “blobs” (Kirsch et al., 1995; Schrader et al., 2004; Saiyed et al., 2007). To characterize potential differences between *Gphn* C4 isoforms in the absence of abnormal cytosolic aggregates, we developed a system to express low amounts of fluorophore-tagged *Gphn* in individual glutamatergic hippocampal neurons. Recombinant adeno-associated viruses (rAAVs) encapsidate single-stranded DNA and require the slow process of complementary-strand synthesis for transgene expression (McCarty et al., 2001). Therefore, we expected that cytosolic *Gphn* aggregation could be minimized by using rAAV-mediated infection.

For single-cell analysis, dissociated hippocampal cultures were transfected with the recombinase Flpo and a cytosolic fluorescent protein (monomeric “ox” blue fluorescent protein, moxBFP) to fill the entire cell. The expression of this construct was restricted to glutamatergic cells through the use of the CamKII α promoter (Wang et al., 2013). Next, Flp-dependent mScarlet-tagged *Gphn* was transduced using recombinant AAV 2/1 particles and immunocytochemistry revealed inhibitory presynaptic terminals and postsynaptic receptors (vGAT and GABA $_A$ R γ 2, respectively; Fig. 2a). As expected, mScarlet signals were only detected in moxBFP-IRES-Flpo cells but were absent from cells transfected with moxBFP alone. Only occasionally, we observed few and small cytosolic exogenous mScarlet-*Gphn* aggregates or “blobs” (Fig. 2b). All *Gphn* C4 isoforms showed a clustered expression and regularly colocalized with vGAT and GABA $_A$ R γ 2 clusters.

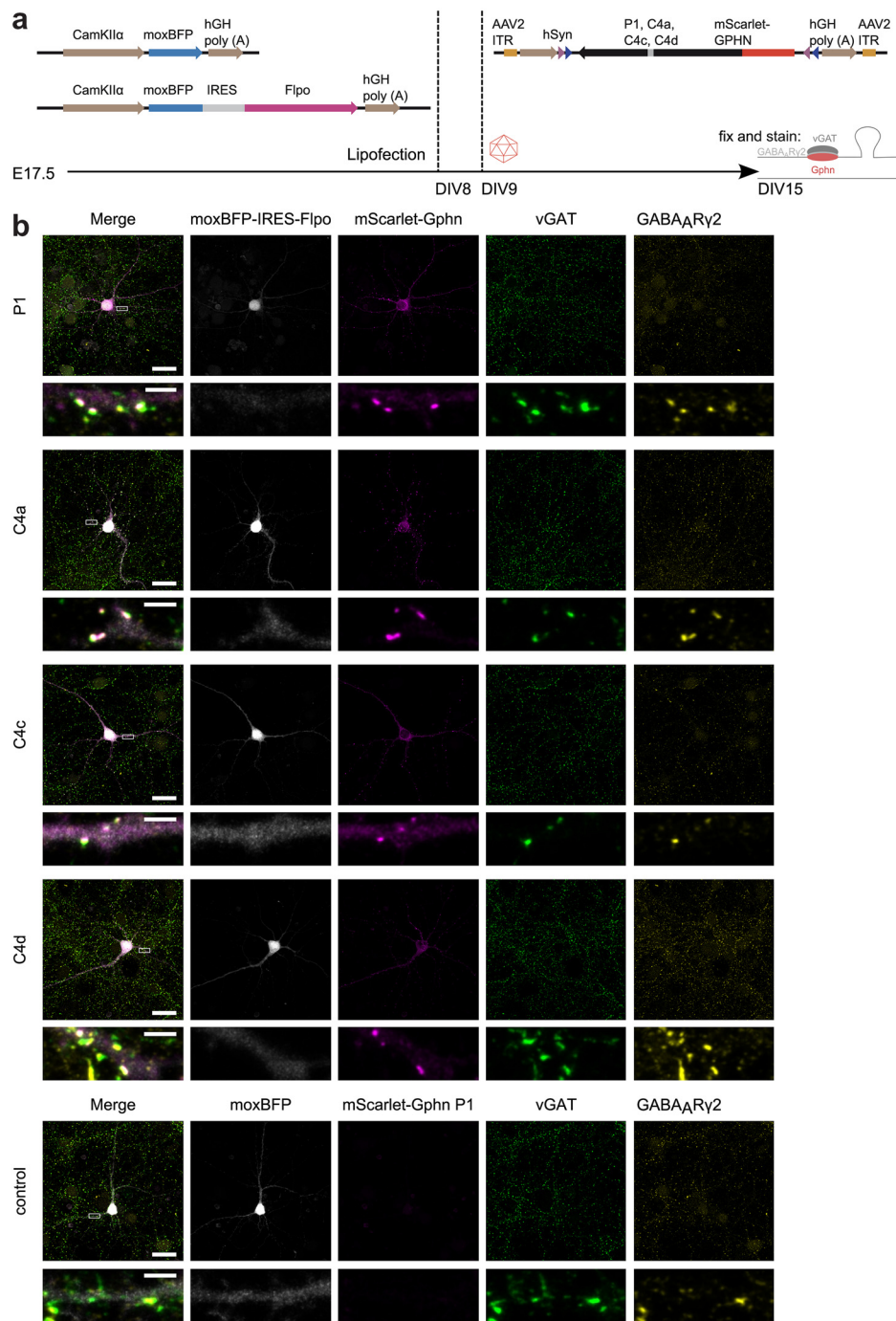


Figure 2. Expression of mScarlet-tagged Gphn C4 isoforms in CamKII α -expressing murine hippocampal neurons. **a**, Hippocampal cultures were transfected after 8 DIV with moxBFP or moxBFP-IRES-Flpo under the control of the CamKII α promoter. After 9 DIV, cultures were infected with adeno-associated virus (AAV) 2/1 carrying Flp dependent mScarlet-tagged Gphn C4 variants as transgene. Cells were immunostained for inhibitory presynaptic terminals (vGAT) and postsynaptic GABA_AR γ 2 after 15 DIV. **b**, Representative confocal images (with adaptive image reconstruction) of neurons expressing moxBFP-IRES-Flpo (or moxBFP as control) and mScarlet-tagged Gphn C4 isoforms. Scale bars: 25 μ m and 2.5 μ m in insets.

To analyze Gphn C4 isoform clustering, we developed an automated and high-content image processing pipeline for image segmentation, intensity measurements, and localization. A total of 11 319 clusters (P1: 2777; C4a: 3187; C4c 2857; C4d: 2498) from 60 cells (15 per condition from three independent cultures) were detected

and analyzed for various parameters. All C4 isoforms showed an average colocalization with GABA_AR γ 2 clusters of \sim 90% and \sim 80% with vGAT clusters. No differences between the isoforms were observed (Fig. 3a,b). Furthermore, neither the size, nor the fluorescence intensity (which is proportional to the number of Gphn

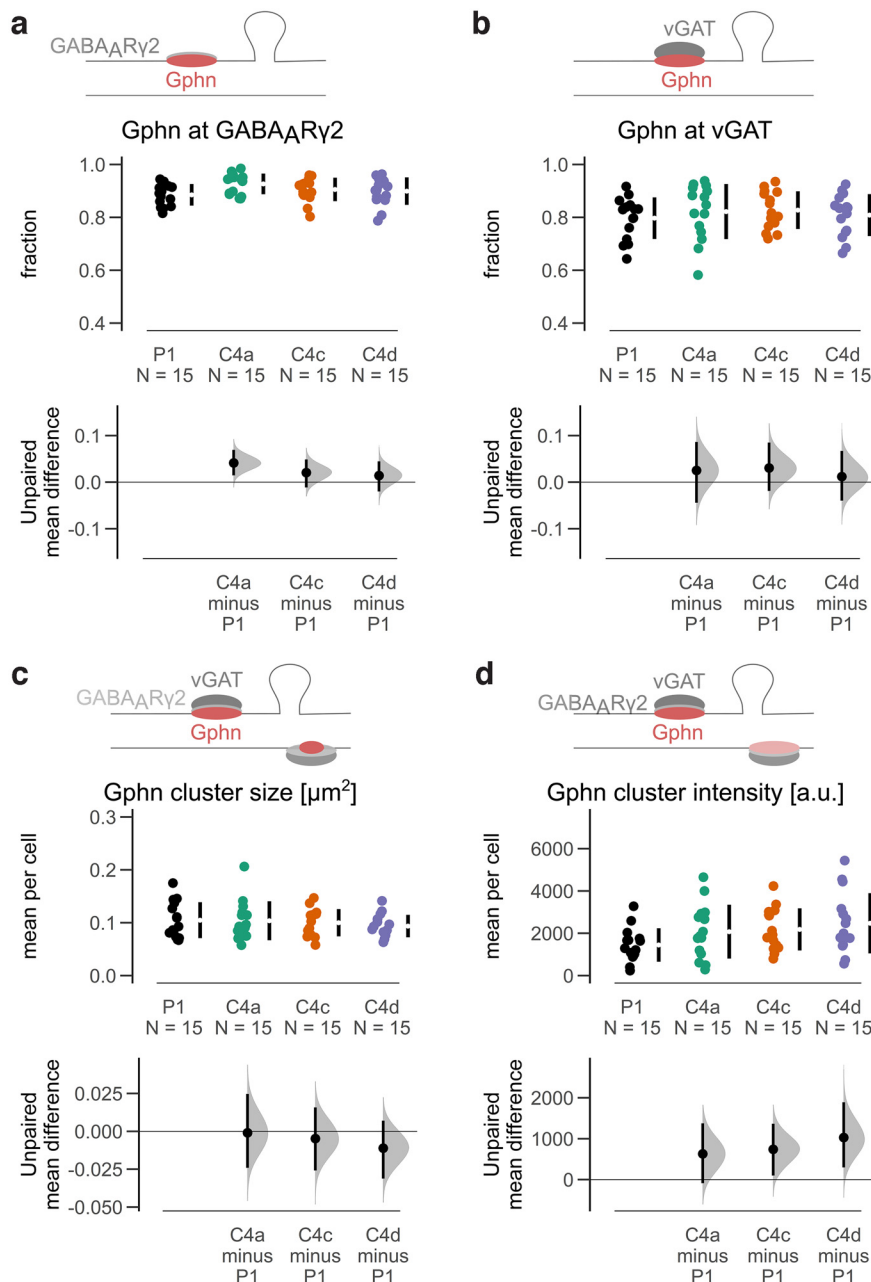


Figure 3. Quantitative analysis of mScarlet-tagged Gphn C4 isoform clusters. **a**, The fraction of GABA_AR γ 2-positive clusters is unchanged between isoforms. ANOVA $F_{(3,56)} = 2.243$, $p = 0.093$. **b**, The fraction of vGAT-positive clusters is indistinguishable between isoforms. ANOVA $F_{(3,56)} = 0.395$, $p = 0.757$. **c**, Gphn cluster sizes (average per cell) of synaptic (vGAT-positive and GABA_AR γ 2-positive) clusters are not different between isoforms. ANOVA $F_{(3,56)} = 0.432$, $p = 0.738$. **d**, Gphn cluster fluorescence intensities (average per cell) of synaptic (vGAT-positive and GABA_AR γ 2-positive) clusters are similar between isoforms. ANOVA $F_{(3,56)} = 2.134$, $p = 0.106$. Each data point represents the mean for an individual neuron. The filled curves indicate the resampled Δ distribution (5000 bootstrap samples) derived from the observed data. The Δ is indicated by the black circle. The 95% confidence interval of the mean difference is illustrated by the black vertical line. See Extended Data Figure 3-1.

molecules) of inhibitory synaptic (vGAT-positive and GABA_AR γ 2-positive) clusters were different among the C4 isoforms (Fig. 3c,d; Extended Data Fig. 3-1a). Additionally, similar numbers of synaptic Gphn clusters per cell area were observed for all C4 isoforms (Extended Data Fig. 3-1b).

Next, we analyzed whether the expression of Gphn C4 isoforms affected GABA_AR clustering. When we selected

synaptic GABA_AR γ 2 clusters (vGAT-positive), larger clusters were observed at Gphn C4a compared with Gphn C4d, while all other comparisons did not reveal differences (Fig. 4a; Extended Data Fig. 4-1a). Additionally, no differences in GABA_AR γ 2 cluster intensities at the different C4 isoform clusters were observed (Fig. 4b; Extended Data Fig. 4-1b). Importantly, the cluster size and cluster intensities of synaptic

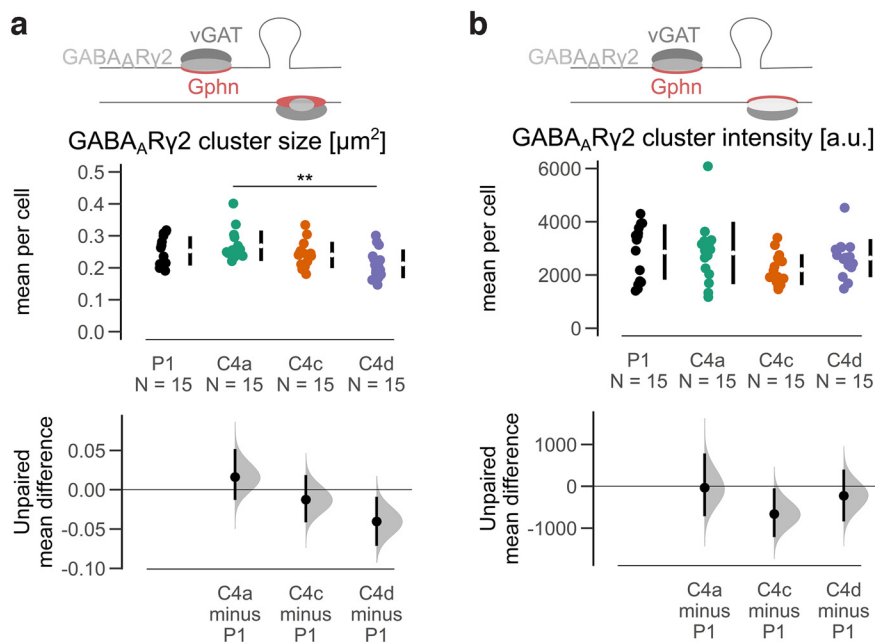


Figure 4. Quantitative analysis of GABA_ARγ2 at mScarlet-tagged Gphn C4 isoform clusters. **a**, GABA_ARγ2 cluster sizes (average per cell) of synaptic (vGAT-positive) clusters are larger at C4a compared with C4d, while all other comparisons are not different between isoforms. Kruskal–Wallis test, $H(3) = 11.18$, $p = 0.011$, pairwise Wilcoxon rank test (Bonferroni corrected); $**p < 0.01$. **b**, GABA_ARγ2 cluster fluorescence intensities (average per cell) of synaptic (vGAT-positive) clusters are similar between isoforms. ANOVA $F_{(3,56)} = 1.687$, $p = 0.180$. Each data point represents the mean for an individual neuron. The filled curves indicate the resampled Δ distribution (5000 bootstrap samples) derived from the observed data. The Δ is indicated by the black circle. The 95% confidence interval of the mean difference is illustrated by the black vertical line. See Extended Data Figure 4-1.

GABA_ARγ2 clusters was increased at all exogenously expressed C4 isoforms compared with endogenous clusters (Extended Data Fig. 4-1c,d).

Altogether, the data show that the basic scaffolding properties and association with GABAergic synapses of C4 isoforms exhibited only minor changes by C4 cassette insertion in cultured hippocampal glutamatergic neurons. The size of GABA_ARγ2 clusters at Gphn C4a were larger compared with clusters at C4d.

Exogenous Gphn C4c clusters are more distally localized

To investigate the cellular distribution of synaptic Gphn clusters (vGAT-positive), we measured their distances to the neuron's center. We observed significantly larger distances for isoform C4c compared with P1 and C4a, while the difference between C4c and C4d was not significant (Fig. 5a). In agreement with this, larger distances were detected for GABA_ARγ2 clusters localized at isoform C4c compared with P1 and C4a, while the difference between C4c and C4d was not statistically significant (Extended Data Fig. 5-1a).

To characterize this effect in more detail, synaptic Gphn clusters were classified according to their distance from the neuron's center: 20 μm radius (somatic and perisomatic clusters), 20 to 40 μm radius and >40 μm radius (distally located clusters). The analysis revealed that the fraction of synaptic clusters at these distances differed for the Gphn isoforms (mixed two-way ANOVA, $p < 0.01$). Specifically, the fraction of synaptic clusters was reduced for C4c versus C4a for the somatic and perisomatic

clusters ($r < 20$ μm) and increased for C4c versus P1 and C4a for distally located clusters ($r > 40$ μm; Fig. 5b). When the effect was analyzed at each isoform, the fraction of synaptic P1 clusters showed no difference between the distances. Synaptic C4a clusters showed a higher fraction of perisomatic clusters ($r < 20$ μm) and distally located clusters ($r > 40$ μm) compared with the intermediate location (20–40 μm). Both synaptic C4c and C4d clusters showed a higher fraction of distally located clusters ($r > 40$ μm) compared with the other locations (Extended Data Fig. 5-1b).

Collectively, Gphn C4 isoforms localized differently in neurons. Here, the presence of a 14-residue sequence encoded by the C4c splice cassette in the C-domain resulted in clusters that were localized further away from the neuron's center than clusters of P1 and C4a isoforms, while Gphn C4d displayed an intermediate behavior.

Reduced localization of Gphn C4c at synaptic P1 clusters

We conducted our exogenous C4 isoform analyses in dissociated murine glutamatergic hippocampal neurons that express Gphn P1 as most abundant variant (Fig. 1b; Dos Reis et al., 2022). In order to directly compare the neuronal localization and scaffolding properties between P1 and C4 isoforms containing one of the C4 cassettes within the same neuron, we extended our imaging system by simultaneously expressing differently tagged Gphn P1 and Gphn C4 isoforms. With this setup, we assessed whether the introduction of sequences encoded by the

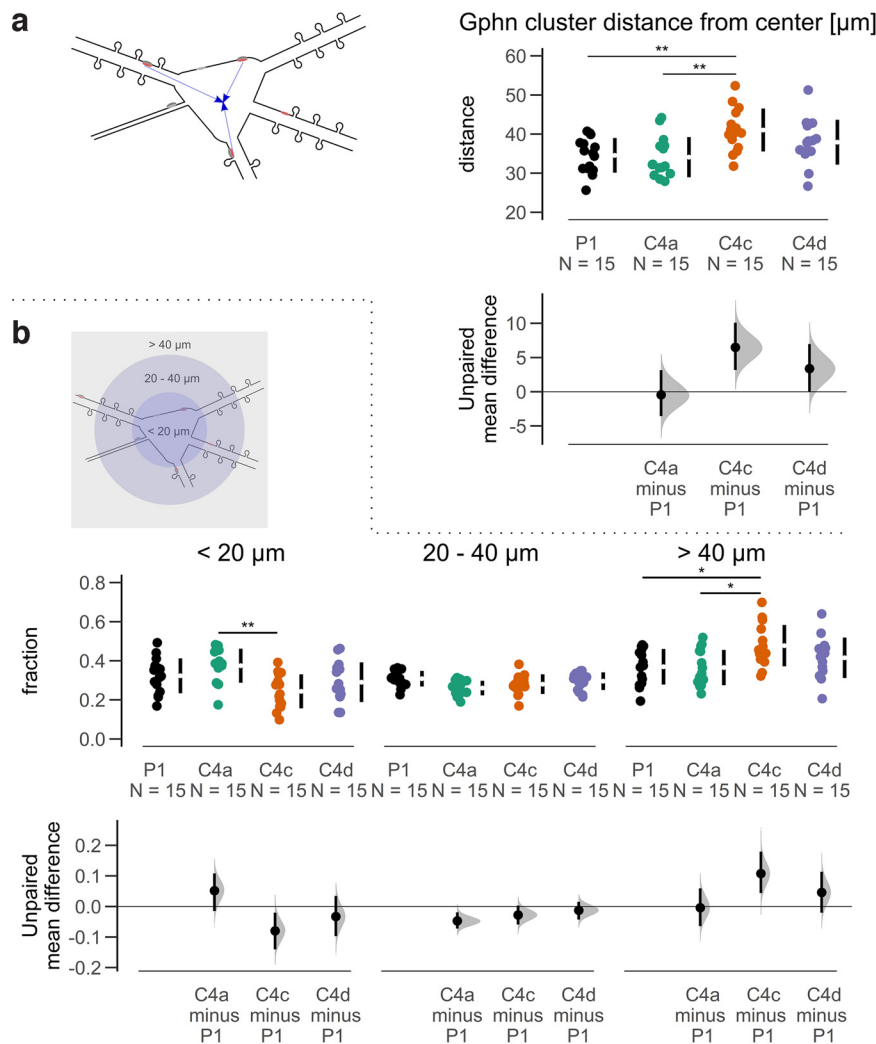


Figure 5. Quantitative analysis of mScarlet-tagged Gphn cluster distances. **a**, Distances of synaptic (vGAT-positive) clusters from the center of the neuron’s soma are increased for isoform C4c compared with P1 and C4a ANOVA $F_{(3,56)} = 5.783$, $p = 0.002$, Tukey’s *post hoc* test; $**p < 0.01$. **b**, Fraction of synaptic (vGAT-positive and GABA_AR γ 2-positive) clusters are increased for C4a versus C4c or C4d at a radius of 20 μm and increased for C4c versus P1 or C4a at a radius >40 μm around the neuron’s center. Data were analyzed with a two-way mixed ANOVA. There was a statistically significant two-way interaction between Gphn isoform and distance on fraction of synaptic clusters, $F_{(4,74)} = 4.683$, $p = 0.002$. Considering the Bonferroni adjusted p -values, the simple main effect of Gphn isoform was significant at <20 μm ($p = 0.006$) and >40 μm ($p = 0.024$) but not at 20–40 μm ($p = 0.057$). Pairwise comparisons show that the mean fraction of synaptic clusters was significantly different in C4a versus C4c ($p = 0.0014$) comparison at <20 μm ; in P1 versus C4c ($p = 0.0233$) and in C4a versus C4c ($p = 0.0168$) at <40 μm . $**p < 0.01$, $*p < 0.05$. Each data point represents the mean for an individual neuron. The filled curves indicate the resampled Δ distribution (5000 bootstrap samples) derived from the observed data. The Δ is indicated by the black circle. The 95% confidence interval of the mean difference is illustrated by the black vertical line. See Extended Data Figure 5-1.

individual C4 cassettes either change the properties of P1 or whether C4 isoforms are equally well recruited to P1 clusters. Analogous to our previous approach, single CamKII α -expressing hippocampal neurons were filled with moxBFP and subsequently infected with AAV2/1 to express mEGFP-tagged Gphn P1 together with one mScarlet-tagged Gphn C4 isoform (Fig. 6a). As expected, mScarlet and mEGFP signals were only detected in moxBFP-IRES-Flpo cells and absent from moxBFP-transfected cells (Fig. 6b).

To detect potential differences, we employed our automated imaging analyses. A total of 7026 (P1: 1287; C4a:

2017; C4c 1939; C4d: 1783) synaptic (vGAT-positive) mEGFP-tagged Gphn P1 clusters from 60 cells (15 per condition from three independent cultures) were inspected. First, we studied whether P1 clustering was affected by additional C4 isoform expression. Neither cluster size nor intensity of mEGFP-Gphn P1 was altered in the presence of mScarlet-Gphn P1, C4a, C4c, or C4d (Fig. 7a,b). Next, we quantified splice variant fluorescence intensity at synaptic P1 clusters. Here, we discovered that C4c intensity at P1 clusters was significantly and strongly reduced (ANOVA effect size, $\eta^2 = 0.3277$) compared with all other conditions (Fig. 7c). This reduction

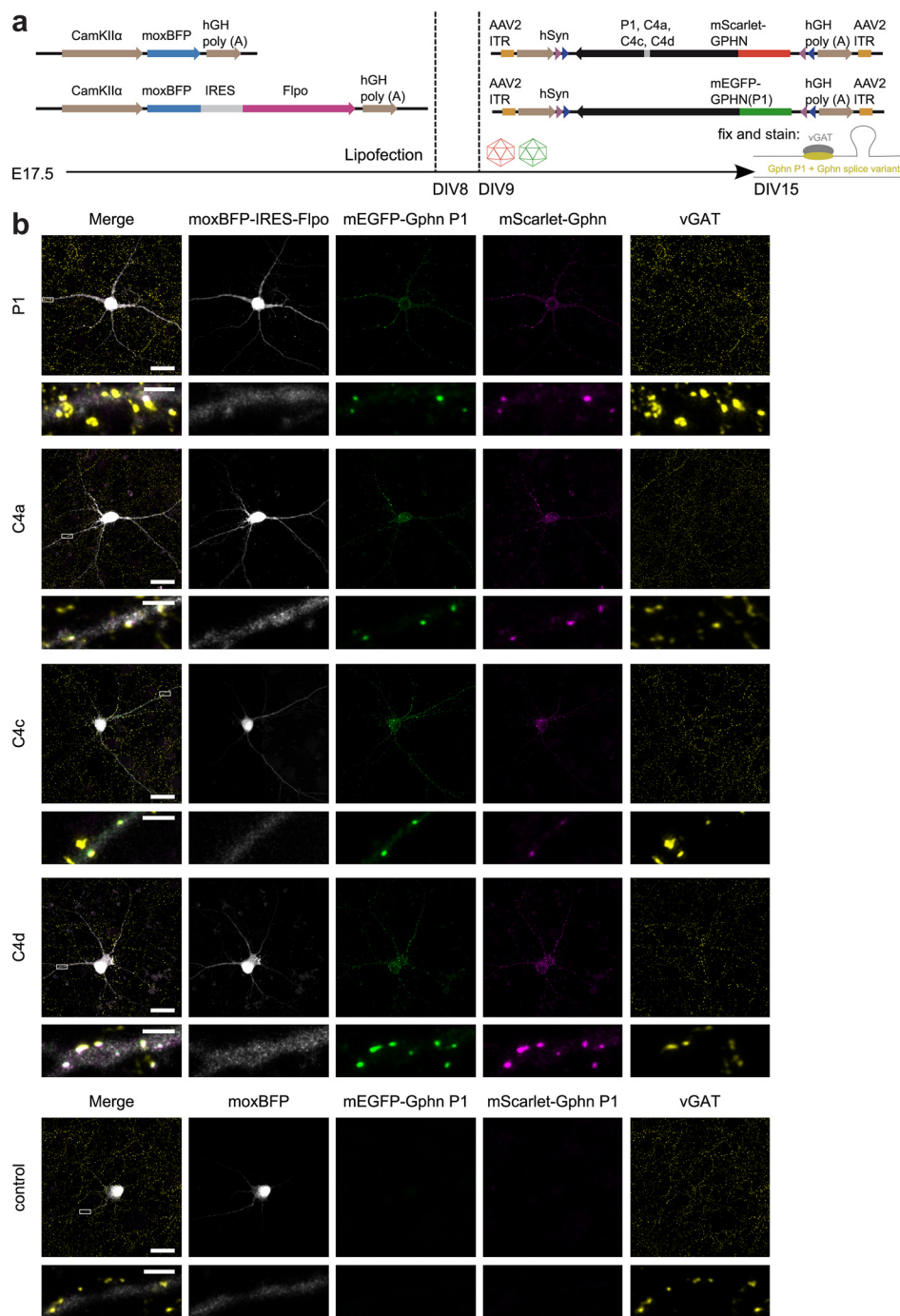


Figure 6. Co-expression of mEGFP-tagged Gphn P1 and mScarlet-tagged Gphn C4 isoforms in CamKII α -expressing murine hippocampal neurons. **a**, Hippocampal cultures were transfected after 8 DIV with moxBFP or moxBFP-IRES-Flpo under the control of the CamKII α promoter. After 9 DIV, cultures were transduced with adeno-associated virus (AAV) 2/1 carrying Flp-dependent mEGFP-tagged Gphn P1 and mScarlet-tagged Gphn C4 variants as transgenes, respectively. **b**, Representative confocal images (with adaptive image reconstruction) of neurons expressing moxBFP-IRES-Flpo (or moxBFP as control), mEGFP-tagged Gphn P1 and mScarlet-tagged Gphn C4 isoforms. Scale bars: 25 μ m and 2.5 μ m in insets.

in C4c fluorescence intensity at P1 clusters was not because of overall reduced cluster size or cluster intensity (Extended Data Fig. 7-1a; Fig. 7d) and is in agreement with the findings that Gphn C4c was enriched at distal synapses (Fig. 3c,d), showing that C4 cassette insertion did not affect cluster size and

intensity when fluorescently labeled isoforms were expressed individually.

Together, our results imply that the subcellular distribution of Gphn C4c shows differences from the other C4 isoforms. On average, fewer Gphn C4c molecules get recruited to P1 predominating clusters. The fluorescence

intensities of the corresponding isoforms at each individual synaptic cluster demonstrate this relationship in detail. Spearman correlation analysis revealed monotonic relationships between mEGFP and mScarlet fluorescence intensities. Highest correlation coefficients were obtained for P1 $\rho = 0.92$ (95% CI [0.91–0.93]) and C4a $\rho = 0.92$ (95% CI [0.91–0.93]), while the coefficient for C4d was smaller $\rho = 0.86$ (95% CI [0.84–0.87]) and the smallest for C4c $\rho = 0.78$ (95% CI [0.75–0.80]; Extended Data Fig. 7-1b). Overall, these results suggest that while all C4 isoforms can colocalize with synaptic P1 clusters, C4c molecules were the least abundant at these sites.

Functional differences in inhibitory signaling between Gphn P1 and Gphn C4c

Our previous experiments suggested that Gphn P1 and Gphn C4c localized differently in cultured hippocampal glutamatergic neurons. We postulated that these gephyrin isoforms might differentially associate with distinct types of GABAergic synapses. GABA_AR α subunits have been shown to localize to distinct sites. For example, GABA_AR $\alpha 1$ predominates at dendritic and somatic synapses, while GABA_AR $\alpha 2$ is found at the axon initial segment (Nusser et al., 1996; Nyíri et al., 2001). However, when we analyzed GABA_AR $\alpha 1$ cluster size and intensity at Gphn P1 and Gphn C4c clusters, no differences were detected (Extended Data Fig. 8-1a–c). Similarly, no differences were observed for GABA_AR $\alpha 2$ cluster size and intensity at either Gphn isoform (Extended Data Fig. 8-1d,e).

Since cluster size and cluster intensities of synaptic GABA_AR $\gamma 2$ clusters were increased at exogenous Gphn clusters (Extended Data Fig. 4-1c,d), we next tested whether inhibitory currents were affected. Current-clamp recordings showed that the cultured neurons could generate overshooting Na⁺-mediated action potentials, indicating their healthy physiological state (Fig. 8a). When action potentials (by TTX) and glutamatergic receptors (by DL-AP5 and CNQX) were blocked, we observed spontaneous miniature IPSCs (mIPSCs; Fig. 8b). A quantitative analysis revealed that neither mIPSC frequency nor mIPSC amplitude were different between Gphn P1 and Gphn C4c expressing cells (Fig. 8c,d). These results are in agreement with our immunocytochemistry staining, which showed no difference in GABA_AR $\gamma 2$ clustering and no change in Gphn cluster density between P1 and C4c (Fig. 4a,b; Extended Data Fig. 3-1b). Interestingly, mIPSCs displayed different kinetics, as revealed by faster decay rates in Gphn C4c versus Gphn P1-expressing cells (Fig. 8e).

In summary, while Gphn P1 and C4c did not differentially associate with GABA_AR $\alpha 1$ or GABA_AR $\alpha 2$ clusters, functional experiments revealed that inhibitory currents decayed faster in the presence of Gphn C4c compared with Gphn P1. These results could be because of the scaffolding of different types of GABA_ARs, the recruitment of additional factors that influence GABA_AR kinetics, or a direct effect of gephyrin clustering on the receptor properties.

Discussion

Alternative splicing contributes to transcriptome and proteome diversity (Lopez Soto et al., 2019). Since the

discovery of Gphn, alternatively spliced transcripts have been reported (Prior et al., 1992; Kirsch et al., 1993; Heck et al., 1997; Ramming et al., 2000; David-Watine, 2001; Rees et al., 2003; Dos Reis et al., 2022). However, for the different neuronal isoforms, functional differences have not been studied in detail. In the SPLICECODE database, Gphn P1 is the most abundant isoform (~62% of all transcripts) in major glutamatergic and GABAergic neurons in hippocampus and cortex (Furlanis et al., 2019). This suggests that Gphn's major function as an inhibitory synaptic scaffolding protein can be fulfilled by P1 and cassette exon splicing generates isoforms with likely modulated properties.

Roughly every 10th transcript (9%) contains the cassette G2 (SPLICECODE database), which alters the protein's trimerization behavior and molybdenum cofactor biosynthesis (Meier et al., 2000; Bedet et al., 2006; Smolinsky et al., 2008). This can be explained by the fact that G2 cassette insertion disrupts α -helix four of the Gphn G-domain (Prior et al., 1992; Schwarz et al., 2001; Sola et al., 2001). In neurons, Gphn G2 can act in a dominant-negative fashion on GlyR clustering, possibly because of its reduced ability to trimerize (Bedet et al., 2006). Therefore, it is conceivable that G2 cassette exon splicing regulates Gphn scaffold remodeling and could contribute to the formation of structurally dynamic postsynaptic clusters.

The presence of ~1% C3-containing transcripts (SPLICECODE database) could be because of imperfect NOVA splicing (Ule et al., 2003; Licatalosi et al., 2008). In addition, previous reports have associated Gphn C3 with non-neuronal expression and molybdenum cofactor biosynthesis (Ramming et al., 2000; Rees et al., 2003; Paarmann et al., 2006; Smolinsky et al., 2008; Nawrotzki et al., 2012). In fact, in the SPLICECODE database, no evidence for C3 expression in CamKII-expressing neurons was detected and transcript levels were low in the other neuronal cell types. Furthermore, C3 was not expressed in glia-free cortical primary neurons, while abundant in neuron-free glia cultures (Smolinsky et al., 2008).

The remaining 28% of transcripts differ in their C4 cassettes, with the majority of transcripts containing C4a (20%) and minor amounts having C4c (3%) or C4d (5%) incorporated (SPLICECODE database). This implies that the majority of neuronal alternatively spliced gephyrin transcripts are generated through differential incorporation of C4 cassettes. These insertions might provide additional protein-protein binding sites, change binding affinities, or alter the structure, thereby modifying the function of the protein isoforms.

The C4a cassette translates into 19 residues (Heck et al., 1997). In a recent study, where exogenous gephyrin was already introduced at DIV1 into cultured hippocampal neurons, increased cluster sizes were observed for a C4a-containing construct compared with P1 (Dos Reis et al., 2022). In contrast, our analysis of synaptic clusters did not reveal such differences between the two isoforms. A major difference between the two experimental approaches is the time point of exogenous Gphn expression. Based on our analysis of endogenous C4 transcript expression, we introduced exogenous Gphn at a time when endogenous

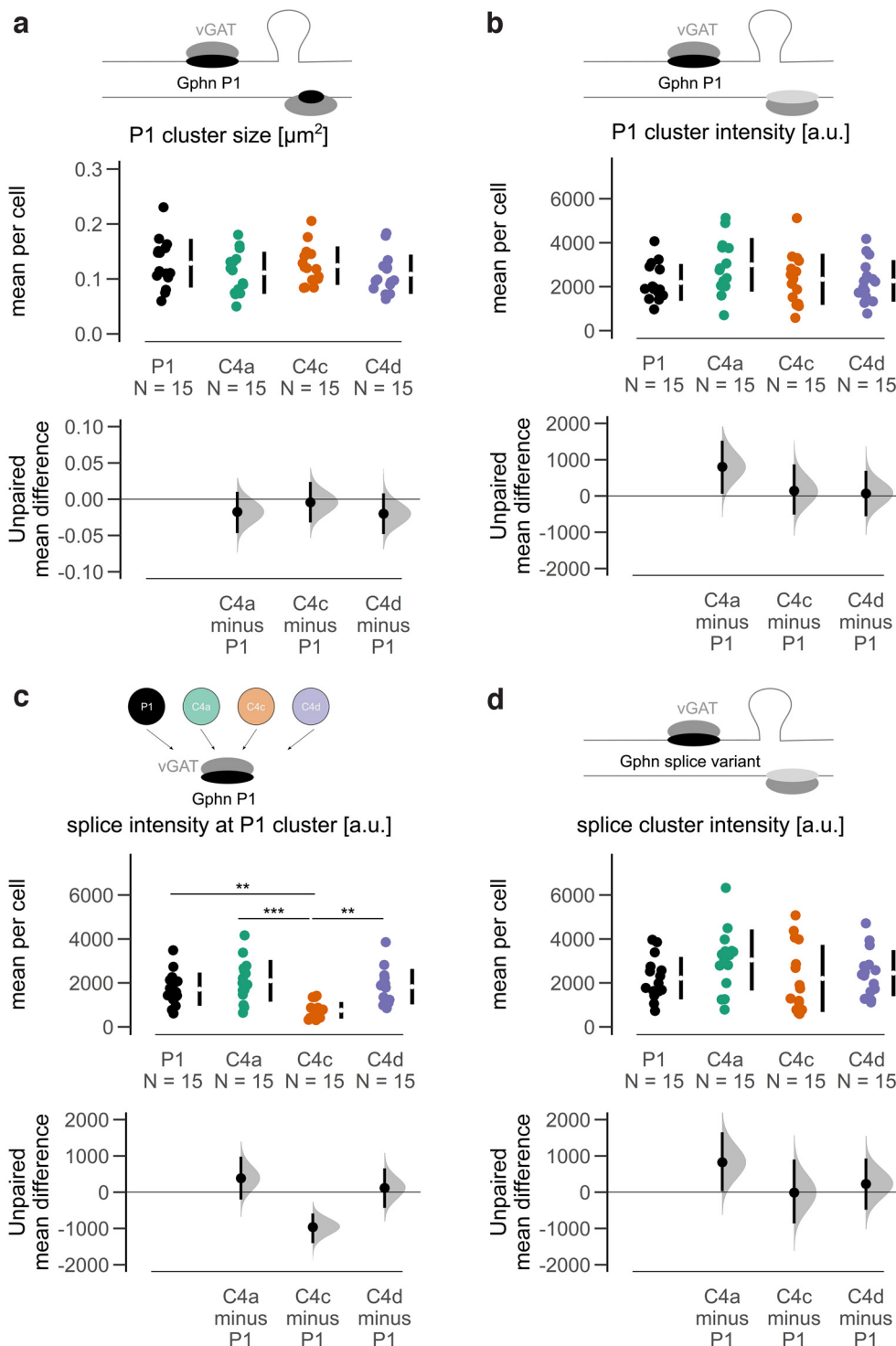


Figure 7. Quantitative analysis of simultaneously expressed mEGFP-tagged Gphn P1 and mScarlet-tagged Gphn C4 isoforms. **a**, Cluster sizes (average per cell) of synaptic (vGAT-positive) P1 clusters are not affected by isoform co-expression. ANOVA $F_{(3,56)} = 0.967$, $p = 0.415$. **b**, Cluster fluorescence intensities (average per cell) of synaptic (vGAT-positive) P1 clusters remain unchanged by isoform co-expression. ANOVA $F_{(3,56)} = 1.856$, $p = 0.148$. **c**, Cluster fluorescence intensities (average per cell) of synaptic (vGAT-positive) Gphn C4c is reduced at P1 clusters compared with all other isoforms. ANOVA $F_{(3,56)} = 9.099$, $p < 0.001$, Tukey's *post hoc* test; $**p < 0.01$, $***p < 0.001$. **d**, Cluster fluorescence intensities (average per cell) of synaptic (vGAT-positive) C4 isoform clusters remain unchanged by P1 co-expression. ANOVA $F_{(3,56)} = 1.467$, $p = 0.233$. Each data point represents the mean for an individual neuron. The filled curves indicate the resampled Δ distribution (5000 bootstrap samples) derived from the observed data. The Δ is indicated by the black circle. The 95% confidence interval of the mean difference is illustrated by the black vertical line. See Extended Data Figure 7-1.

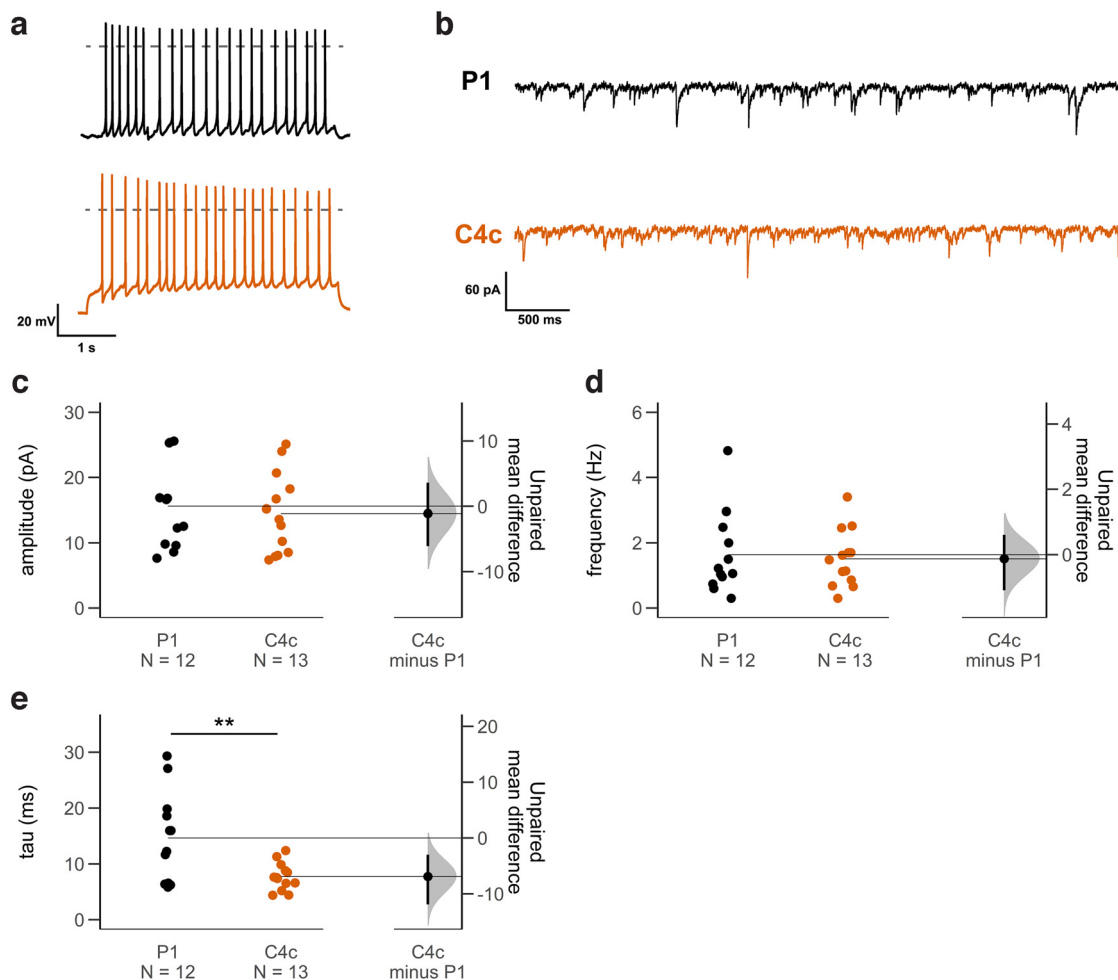


Figure 8. Analysis of miniature IPSCs (mIPSCs) in cultured hippocampal neurons expressing either mScarlet-tagged Gphn P1 or C4c. P1 (black), C4c (orange). **a**, Current-clamp recordings showing the firing activity of cultured neurons during a 2 s depolarizing current pulse. The dashed lines indicate 0 mV. **b**, Example voltage clamp recordings of mIPSCs from either splice variant. **c–e**, Estimation plots for mIPSC amplitude, frequency, and decay of P1 and C4c splice variants. **c**, There was no significant difference in mIPSC amplitudes between P1 and C4c splice variants [P1: 15.6 ± 1.9 pA, C4c: 14.5 ± 1.7 pA; $N_{P1} = 12$, $N_{C4c} = 13$; unpaired mean difference ($\Delta C4c-P1$): -1.1 pA; 95% CI $[-6.1-3.7]$; $p_{P1/C4c} = 0.68$ (two-sided permutation test)]. **d**, There was no significant difference in mIPSC frequencies [P1: 1.6 ± 0.4 Hz, C4c: 1.5 ± 0.2 Hz; $N_{P1} = 12$, $N_{C4c} = 13$; unpaired mean difference ($\Delta C4c-P1$): -0.1 Hz; 95% CI $[-1.1-0.6]$; $p_{P1/C4c} = 0.78$ (two-sided permutation test)]. **e**, The decay time constants of the mIPSCs were shorter in C4c compared with P1 [P1: 14.6 ± 2.3 ms, C4c: 7.7 ± 0.7 ms; $N_{P1} = 12$, $N_{C4c} = 13$; unpaired mean difference ($\Delta C4c-P1$): -6.9 ms; 95% CI $[-12.1--3.0]$; $p_{P1/C4c} = 0.0056$ (two-sided permutation test)]; $**p < 0.01$. Each data point represents the mean of a 50 s recording interval of an individual neuron. The filled curves indicate the resampled Δ distribution (5000 bootstrap samples) derived from the observed data. The Δ is indicated by the black circle, which is horizontally aligned with the mean of the test group. The 95% confidence interval of the mean difference is illustrated by the black vertical line. All recordings were performed at 12–15 DIV. During the voltage clamp recordings, glutamatergic input was blocked by CNQX and DL-AP5. Na^+ -mediated action potentials were blocked by TTX. Holding potential was -50 mV. See Extended Data Figure 8-1.

expression had already plateaued. Additionally, our transcript analysis suggested that C4a-containing transcripts are expressed later than C4-lacking ones. Therefore, it is possible that cluster formation is altered if the sequence of expression is reversed (Dos Reis et al., 2022).

Three different residues within the 14 amino acid long C4c cassette can be phosphorylated; in a bioinformatic prediction, multiple kinases such as PKA, PKC, CamKII, GSK3, RSK, and cdc2 have been identified as potential candidates (Herweg and Schwarz, 2012). The introduction of additional phosphorylation sites into gephyrin's C-domain

could add an extra regulatory layer. Phosphorylation at various sites in the central domain have been associated with structural remodeling of GABAergic synapses (Tyagarajan et al., 2011, 2013; Flores et al., 2015). Therefore, it could be postulated that phosphorylation of a less abundant isoform, such as C4c, could affect GABAergic synapse plasticity in a very distinct context or at a subset of specific synapses. Recombinantly produced proteins P1 and C4c showed similar oligomerization behavior and binding affinities for the GlyR β -loop (Herweg and Schwarz, 2012). Our clustering analysis showed that the subcellular localization

and recruitment to clusters with the predominating isoform P1 was strongly reduced for C4c. The localization of synaptic clusters indicates that C4c may preferentially fulfill functions in more distal dendritic regions. This observation is in agreement with the reduced intensities at P1 clusters and implies that P1 and C4c may show differential association with components of the transport machinery. Additionally, faster mIPSC decay rates suggested that GABA_AR function is differently affected by C4c versus P1 scaffolding.

Similarities between the 21 residue C4d sequence and the α -helical dimerization domain 1B of the human keratin 8 were proposed as an additional binding site for protein-protein interactions (Ramming et al., 2000; Rees et al., 2003). In all our analyses, no difference between C4d and P1 clustering was detected. In a recent study, when C4d-containing exogenous gephyrin was already introduced at DIV1, increased cluster size, decreased cluster density, and increased association with GAD-65 were observed (Dos Reis et al., 2022). Similar to the findings for C4a, this suggests that cluster formation can be affected, when the C4d isoform is expressed before the onset of synaptogenesis (Vogel and Marcotte, 2012; Smith et al., 2013; Liu et al., 2016; Aebersold et al., 2018).

Limitations of our study are the exogenous Gphn expression and the use of dissociated cultured hippocampal neurons. While artificial Gphn aggregation, which is well-known in the field, was reduced with our AAV expression system, we still introduced additional transcript copies. These could promote the association of exogenously expressed Gphn molecules to any preexisting synaptic cluster rather than to a specifically-targeted synapse, simply because of increased protein levels. While our P1-targeting approach underline this view, the results demonstrate that C4c-containing variants were less abundant at P1 clusters, which is in line with the preferred distal dendritic localization of this variant.

Regarding a second limitation, dissociated neuron cultures may not retain their full set of naturally occurring synaptic partners. For instance, different types of interneurons can preferentially form synapses in specific regions of the postsynaptic neuron; SST-expressing neurons predominantly from synapses on dendrites, while parvalbumin-expressing neurons form synapses in the perisomatic region (Tremblay et al., 2016; Contreras et al., 2019). While some aspects of subcellular postsynaptic protein localization can occur in a cell autonomous fashion, i.e., in dissociated cultures, others may only be achieved when the correct anatomic input-specificity is preserved, i.e., *in vivo*.

Importantly, in our experimental paradigm, exogenous Gphn expression started roughly after DIV11, which is later than the onset of synaptogenesis (Deng et al., 2007; Grabrucker et al., 2009). Therefore, our observations relate to the scaffolding of Gphn isoforms in neurons with preexisting inhibitory synapses and no conclusions can be made about the impact of C4 alternative splicing on synaptogenesis. To advance our knowledge about the functional impact of C4 splicing, analyses of the scaffolding behavior of endogenously expressed gephyrin C4 isoform are needed. Here, a genetic deletion of

individual C4 cassettes is needed, which is similar to an approach that was recently performed for an alternatively spliced exon of Neurexin 3 (Hauser et al., 2022). In addition, the use of neurons with a complete deletion of endogenous Gphn and subsequent expression of individual Gphn variants will further isolate functions of each Gphn splice variants.

Overall, cassette exon splicing of the C4 cluster occurred in GABAergic and glutamatergic neurons of the hippocampus and cortex (SPliceCODE dataset) and other studies have suggested that this is predominantly a neuron-specific process (Ramming et al., 2000; Rees et al., 2003; Paarmann et al., 2006; Smolinsky et al., 2008). Exogenously expressed C4 isoforms in glutamatergic dissociated neurons demonstrated, for the most part, redundant scaffolding behavior, while localization and functional differences for C4c-containing isoforms suggest that C4 cassette splicing can indeed contribute to inhibitory synapse heterogeneity.

References

- Aebersold R, et al. (2018) How many human proteoforms are there? *Nat Chem Biol* 14:206–214.
- Bedet C, Bruusgaard JC, Vergo S, Groth-Pedersen L, Eimer S, Triller A, Vannier C (2006) Regulation of gephyrin assembly and glycine receptor synaptic stability. *J Biol Chem* 281:30046–30056.
- Belaidi AA, Schwarz G (2013) Metal insertion into the molybdenum cofactor: product-substrate channelling demonstrates the functional origin of domain fusion in gephyrin. *Biochem J* 450:149–157.
- Contreras A, Hines DJ, Hines RM (2019) Molecular specialization of GABAergic synapses on the soma and axon in cortical and hippocampal circuit function and dysfunction. *Front Mol Neurosci* 12:154.
- David-Watine B (2001) The human gephyrin (GPHN) gene: structure, chromosome localization and expression in non-neuronal cells. *Gene* 271:239–245.
- Dejanovic B, Lal D, Catarino CB, Arjune S, Belaidi AA, Trucks H, Vollmar C, Surges R, Kunz WS, Motameny S, Altmüller J, Köhler A, Neubauer BA, Epicure Consortium, Nürnberg P, Noachtar S, Schwarz G, Sander T (2014a) Exonic microdeletions of the gephyrin gene impair GABAergic synaptic inhibition in patients with idiopathic generalized epilepsy. *Neurobiol Dis* 67:88–96.
- Dejanovic B, Semtner M, Ebert S, Lamkemeyer T, Neuser F, Lüscher B, Meier JC, Schwarz G (2014b) Palmitoylation of gephyrin controls receptor clustering and plasticity of GABAergic synapses. *PLoS Biol* 12:e1001908.
- Deng L, Yao J, Fang C, Dong N, Luscher B, Chen G (2007) Sequential postsynaptic maturation governs the temporal order of GABAergic and glutamatergic synaptogenesis in rat embryonic cultures. *J Neurosci* 27:10860–10869.
- Dotd HU, Ziegglänsberger W (1994) Infrared videomicroscopy: a new look at neuronal structure and function. *Trends Neurosci* 17:453–458.
- Dos Reis R, Kornobis E, Pereira A, Tores F, Carrasco J, Gautier C, Jahannault-Talignani C, Nitschké P, Muchardt C, Schlosser A, Maric HM, Ango F, Allemand E (2022) Complex regulation of Gephyrin splicing is a determinant of inhibitory postsynaptic diversity. *Nat Commun* 13:3507.
- Feng G, Tintrup H, Kirsch J, Nichol MC, Kuhse J, Betz H, Sanes JR (1998) Dual requirement for gephyrin in glycine receptor clustering and molybdoenzyme activity. *Science* 282:1321–1324.
- Flores CE, Nikonenko I, Mendez P, Fritschy JM, Tyagarajan SK, Muller D (2015) Activity-dependent inhibitory synapse remodeling

- through gephyrin phosphorylation. *Proc Natl Acad Sci USA* 112: E65–E72.
- Fritschy JM, Harvey RJ, Schwarz G (2008) Gephyrin: where do we stand, where do we go? *Trends Neurosci* 31:257–264.
- Furlanis E, Traunmüller L, Fucile G, Scheiffle P (2019) Landscape of ribosome-engaged transcript isoforms reveals extensive neuronal-cell-class-specific alternative splicing programs. *Nat Neurosci* 22:1709–1717.
- Grabrucker A, Vaida B, Bockmann J, Boeckers TM (2009) Synaptogenesis of hippocampal neurons in primary cell culture. *Cell Tissue Res* 338:333–341.
- Grosskreutz Y, Betz H, Kneussel M (2003) Rescue of molybdenum cofactor biosynthesis in gephyrin-deficient mice by a *Cnx1* transgene. *Biochem Biophys Res Commun* 301:450–455.
- Hauser DJ, Moss AJ, Rosenzweig C, Jaffe SN, Robinson J, Litman L (2022) Targeted proteoform mapping uncovers specific Neurexin-3 variants required for dendritic inhibition. *Neuron* 110:2094–2109. e10.
- Heck S, Enz R, Richter-Landsberg C, Blohm DH (1997) Expression and mRNA splicing of glycine receptor subunits and gephyrin during neuronal differentiation of P19 cells in vitro, studied by RT-PCR and immunocytochemistry. *Brain Res Dev Brain Res* 98:211–220.
- Herweg J, Schwarz G (2012) Splice-specific glycine receptor binding, folding, and phosphorylation of the scaffolding protein gephyrin. *J Biol Chem* 287:12645–12656.
- Ho J, Tumkaya T, Aryal S, Choi H, Claridge-Chang A (2019) Moving beyond p values: data analysis with estimation graphics. *Nat Methods* 16:565–566.
- Kim YG, Shin JJ, Kim SJ (2021) Minhee analysis package: an integrated software package for detection and management of spontaneous synaptic events. *Mol Brain* 14:138.
- Kimura T, Ferran B, Tsukahara Y, Shang Q, Desai S, Fedoce A, Pimentel DR, Luptak I, Adachi T, Ido Y, Matsui R, Bachschmid MM (2019) Production of adeno-associated virus vectors for in vitro and in vivo applications. *Sci Rep* 9:13601.
- Kirsch J, Malosio ML, Wolters I, Betz H (1993) Distribution of gephyrin transcripts in the adult and developing rat brain. *Eur J Neurosci* 5:1109–1117.
- Kirsch J, Kuhse J, Betz H (1995) Targeting of glycine receptor subunits to gephyrin-rich domains in transfected human embryonic kidney cells. *Mol Cell Neurosci* 6:450–461.
- Licatalosi DD, Mele A, Fak JJ, Ule J, Kayikci M, Chi SW, Clark TA, Schweitzer AC, Blume JE, Wang X, Darnell JC, Darnell RB (2008) HITS-CLIP yields genome-wide insights into brain alternative RNA processing. *Nature* 456:464–469.
- Liu Y, Beyer A, Aebersold R (2016) On the dependency of cellular protein levels on mRNA abundance. *Cell* 165:535–550.
- Lopez Soto EJ, Gandal MJ, Gontopoulos-Pournatzis T, Heller EA, Luo D, Zheng S (2019) Mechanisms of neuronal alternative splicing and strategies for therapeutic interventions. *J Neurosci* 39:8193–8199.
- Moreno Manrique JF, Voit PR, Windsor KE, Karla AR, Rodriguez SR, Beaudoin GMJ (2021) SynapseJ: An automated, synapse identification macro for ImageJ. *Front Neural Circuits* 15:731333.
- McCarty DM, Monahan PE, Samulski RJ (2001) Self-complementary recombinant adeno-associated virus (scAAV) vectors promote efficient transduction independently of DNA synthesis. *Gene Ther* 8:1248–1254.
- Meier J, De Chaldée M, Triller A, Vannier C (2000) Functional heterogeneity of gephyrins. *Mol Cell Neurosci* 16:566–577.
- Nawrotzki R, Islinger M, Vogel I, Völkl A, Kirsch J (2012) Expression and subcellular distribution of gephyrin in non-neuronal tissues and cells. *Histochem Cell Biol* 137:471–482.
- Nusser Z, Sieghart W, Benke D, Fritschy JM, Somogyi P (1996) Differential synaptic localization of two major gamma-aminobutyric acid type A receptor alpha subunits on hippocampal pyramidal cells. *Proc Natl Acad Sci U S A* 93:11939–11944.
- Nyiri G, Freund TF, Somogyi P (2001) Input-dependent synaptic targeting of alpha(2)-subunit-containing GABA(A) receptors in synapses of hippocampal pyramidal cells of the rat. *Eur J Neurosci* 13:428–442.
- O’Sullivan GA, Jedlicka P, Chen HX, Kalbouneh H, Ippolito A, Deller T, Nawrotzki RA, Kuhse J, Kalaidzidis YL, Kirsch J, Schwarzacher SW, Betz H (2016) Forebrain-specific loss of synaptic GABAA receptors results in altered neuronal excitability and synaptic plasticity in mice. *Mol Cell Neurosci* 72:101–113.
- Paarmann I, Schmitt B, Meyer B, Karas M, Betz H (2006) Mass spectrometric analysis of glycine receptor-associated gephyrin splice variants. *J Biol Chem* 281:34918–34925.
- Prior P, et al. (1992) Primary structure and alternative splice variants of gephyrin, a putative glycine receptor-tubulin linker protein. *Neuron* 8:1161–1170.
- Ramming M, Kins S, Werner N, Hermann A, Betz H, Kirsch J (2000) Diversity and phylogeny of gephyrin: tissue-specific splice variants, gene structure, and sequence similarities to molybdenum cofactor-synthesizing and cytoskeleton-associated proteins. *Proc Natl Acad Sci U S A* 97:10266–10271.
- Rees MI, Harvey K, Ward H, White JH, Evans L, Duguid IC, Hsu CC, Coleman SL, Miller J, Baer K, Waldvogel HJ, Gibbon F, Smart TG, Owen MJ, Harvey RJ, Snell RG (2003) Isoform heterogeneity of the human gephyrin gene (GPHN), binding domains to the glycine receptor, and mutation analysis in hyperekplexia. *J Biol Chem* 278:24688–24696.
- Saiyed T, Paarmann I, Schmitt B, Haeger S, Sola M, Schmalzing G, Weissenhorn W, Betz H (2007) Molecular basis of gephyrin clustering at inhibitory synapses: role of G- and E-domain interactions. *J Biol Chem* 282:5625–5632.
- Sander B, Tria G, Shkumatov AV, Kim EY, Grossmann JG, Tessmer I, Svergun DI, Schindelin H (2013) Structural characterization of gephyrin by AFM and SAXS reveals a mixture of compact and extended states. *Acta Crystallogr D Biol Crystallogr* 69:2050–2060.
- Schrader N, Kim EY, Winking J, Paulukat J, Schindelin H, Schwarz G (2004) Biochemical characterization of the high affinity binding between the glycine receptor and gephyrin. *J Biol Chem* 279:18733–18741.
- Schwarz G, Schrader N, Mendel RR, Hecht HJ, Schindelin H (2001) Crystal structures of human gephyrin and plant *Cnx1* G domains: comparative analysis and functional implications. *J Mol Biol* 312:405–418.
- Sheng M, Kim E (2011) The postsynaptic organization of synapses. *Cold Spring Harb Perspect Biol* 3:a005678.
- Smith LM, Kelleher NL, Consortium for Top Down P; Consortium for Top Down Proteomics (2013) Proteoform: a single term describing protein complexity. *Nat Methods* 10:186–187.
- Smolinsky B, Eichler SA, Buchmeier S, Meier JC, Schwarz G (2008) Splice-specific functions of gephyrin in molybdenum cofactor biosynthesis. *J Biol Chem* 283:17370–17379.
- Sola M, Kneussel M, Heck IS, Betz H, Weissenhorn W (2001) X-ray crystal structure of the trimeric N-terminal domain of gephyrin. *J Biol Chem* 276:25294–25301.
- Sola M, Bavro VN, Timmins J, Franz T, Ricard-Blum S, Schoehn G, Ruigrok RW, Paarmann I, Saiyed T, O’Sullivan GA, Schmitt B, Betz H, Weissenhorn W (2004) Structural basis of dynamic glycine receptor clustering by gephyrin. *EMBO J* 23:2510–2519.
- Stallmeyer B, Schwarz G, Schulze J, Nerlich A, Reiss J, Kirsch J, Mendel RR (1999) The neurotransmitter receptor-anchoring protein gephyrin reconstitutes molybdenum cofactor biosynthesis in bacteria, plants, and mammalian cells. *Proc Natl Acad Sci U S A* 96:1333–1338.
- Tremblay R, Lee S, Rudy B (2016) GABAergic interneurons in the neocortex: from cellular properties to circuits. *Neuron* 91:260–292.
- Tyagarajan SK, Ghosh H, Yévenes GE, Nikonenko I, Ebeling C, Schwerdel C, Sidler C, Zeilhofer HU, Gerrits B, Müller D, Fritschy JM (2011) Regulation of GABAergic synapse formation and plasticity by GSK3beta-dependent phosphorylation of gephyrin. *Proc Natl Acad Sci U S A* 108:379–384.
- Tyagarajan SK, Ghosh H, Yévenes GE, Imanishi SY, Zeilhofer HU, Gerrits B, Fritschy JM (2013) Extracellular signal-regulated kinase and glycogen synthase kinase 3β regulate gephyrin postsynaptic

- aggregation and GABAergic synaptic function in a calpain-dependent mechanism. *J Biol Chem* 288:9634–9647.
- Ule J, Jensen KB, Ruggiu M, Mele A, Ule A, Darnell RB (2003) CLIP identifies Nova-regulated RNA networks in the brain. *Science* 302:1212–1215.
- Vogel C, Marcotte EM (2012) Insights into the regulation of protein abundance from proteomic and transcriptomic analyses. *Nat Rev Genet* 13:227–232.
- Wang X, Zhang C, Szábo G, Sun QQ (2013) Distribution of CaMKII α expression in the brain in vivo, studied by CaMKII α -GFP mice. *Brain Res* 1518:9–25.
- Witte H, Schreiner D, Scheiffele P (2019) A Sam68-dependent alternative splicing program shapes postsynaptic protein complexes. *Eur J Neurosci* 49:1436–1453.
- Xu J, DeVries SH, Zhu Y (2020) Quantification of adeno-associated virus with safe nucleic acid dyes. *Hum Gene Ther* 31:1086–1099.